The first copper (II) complex with 1,10-phenanthroline and salubrinal with interesting biochemical properties

S. Masuri[1], E. Cadoni[1], M.G. Cabiddu[1], F. Isaia[1], M.G. Demuru[1], L. Moráň[2,3], D. Buček[2,] P. Vaňhara[2,3], J. Havel[3,4], T. Pivetta[*,1]

[1]Dipartimento di Scienze Chimiche e Geologiche, Università degli Studi di Cagliari, Cittadella Universitaria, 09042 Monserrato CA – Italy; [2]Department of Histology and Embryology, Faculty of Medicine, Masaryk University, Brno, Czech Republic; [3]International Clinical Research Center, St. Anne's University Hospital, Brno, Czech Republic; [4]Department of Chemistry, Faculty of Science, Masaryk University, Brno, Czech Republic.

SUPPLEMENTARY INFORMATION

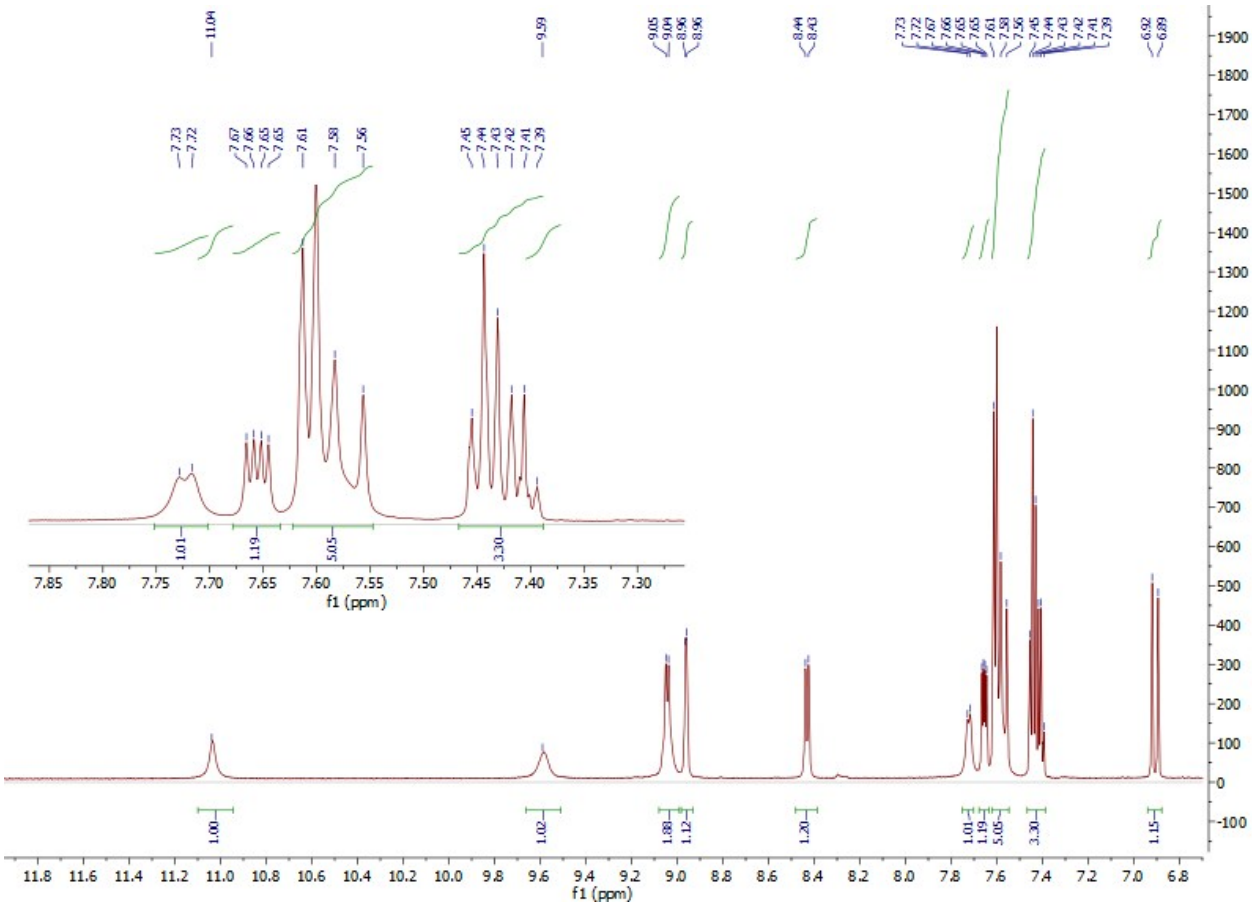

Fig. S1: ^{1}H-NMR spectrum of **SAL** (600 MHz, DMSO d-6).

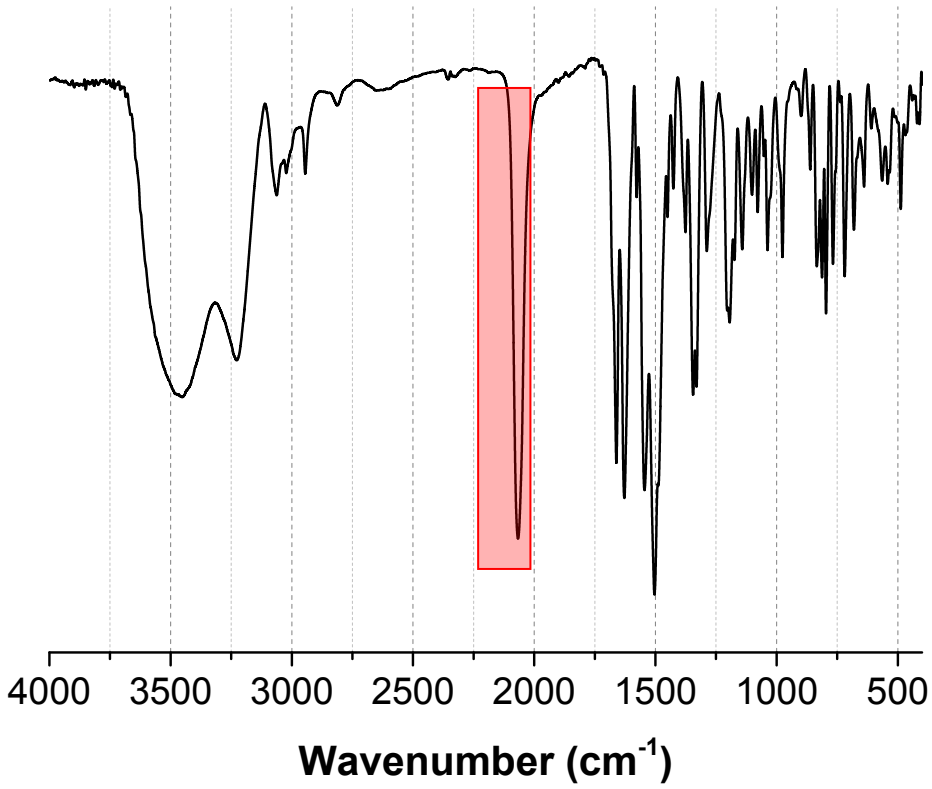

Fig. S2: FT-IR of **SAL** prior to aqueous washing for SCN^- removal. The peak relative to SCN^- at 2070 cm^{-1} is evidenced.

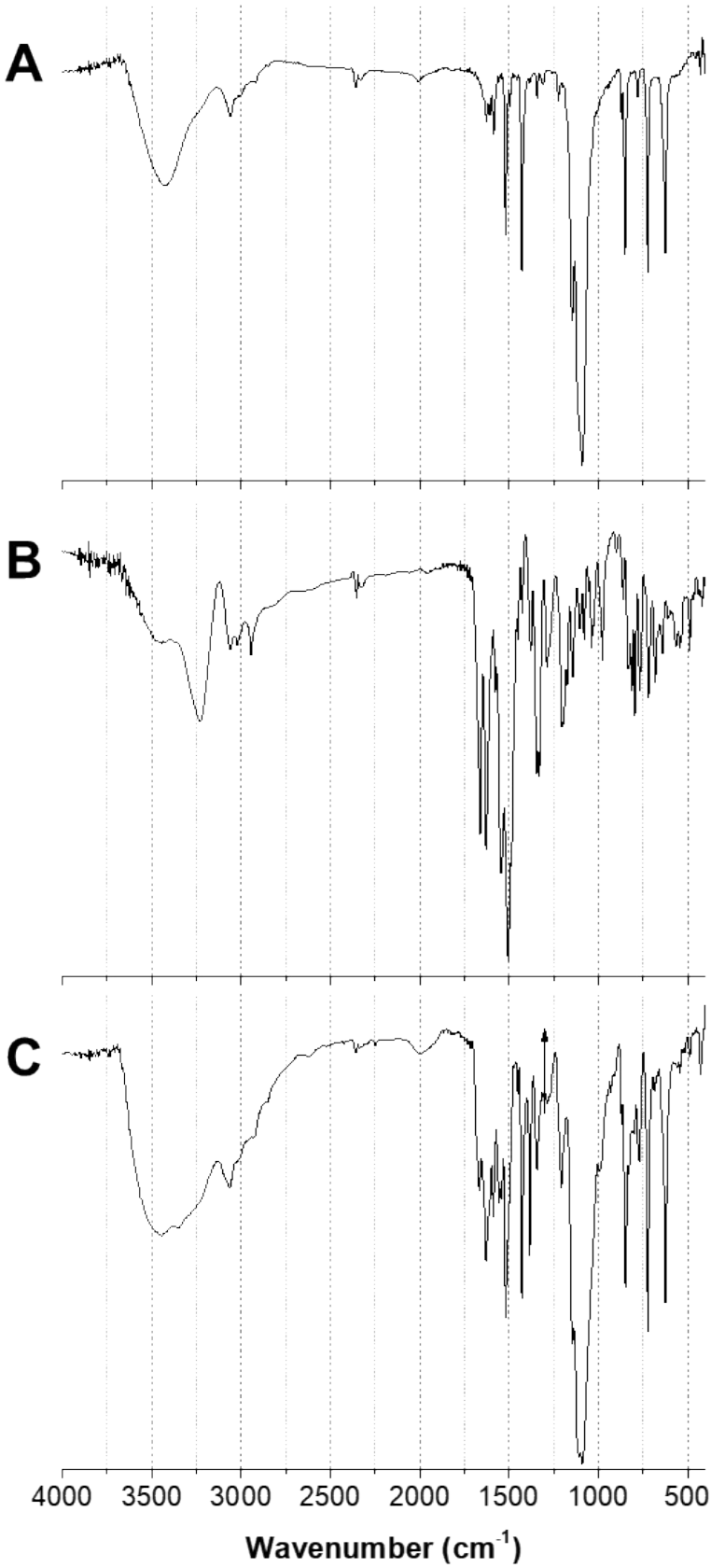

Fig. S3: IR spectra of C0 (**A**), SAL (**B**) and $[Cu(phen)_2(SAL)](ClO_4)_2$ (**C**)

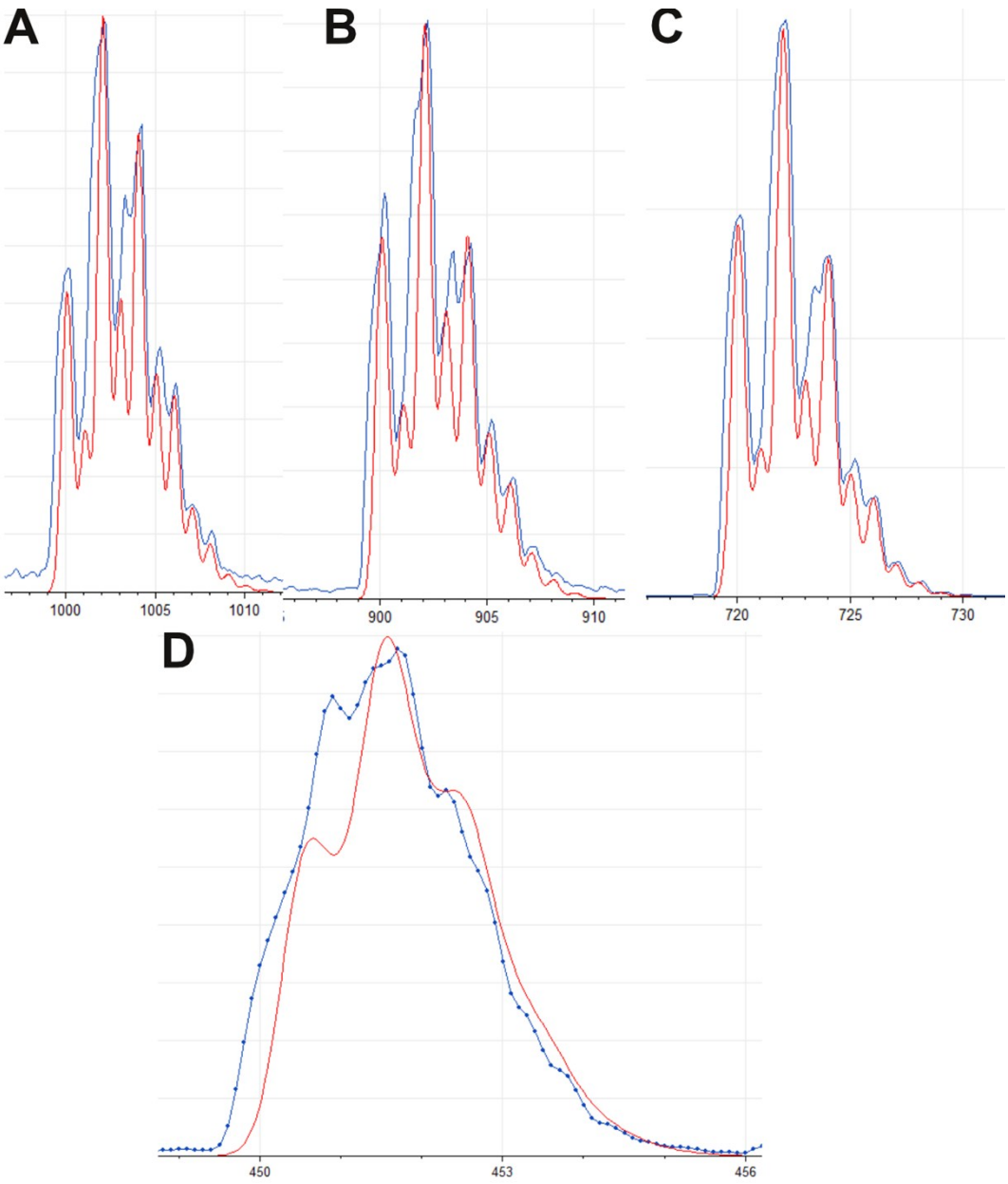

Fig. S4: Experimental (blue line) and calculated (red line) isotopic patterns of the peaks at *m/z* (**A**) 1002-1000 ($[Cu(phen)_2(SAL)(ClO_4)]^+$), (**B**) 902-900 ($[Cu(phen)_2(SAL\text{-}H)]^+$), (**C**) 722-720 ($[Cu(phen)(SAL\text{-}H)]^+$), (**D**) 450.5 ($[Cu(phen)_2(SAL)]^{2+}$).

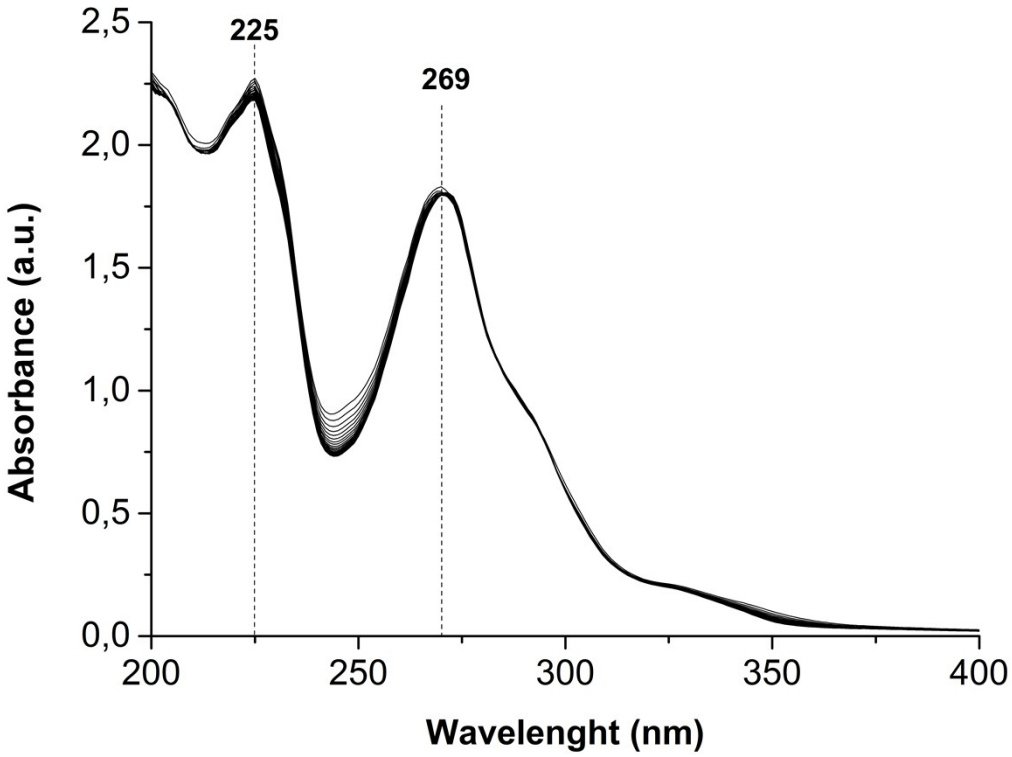

A

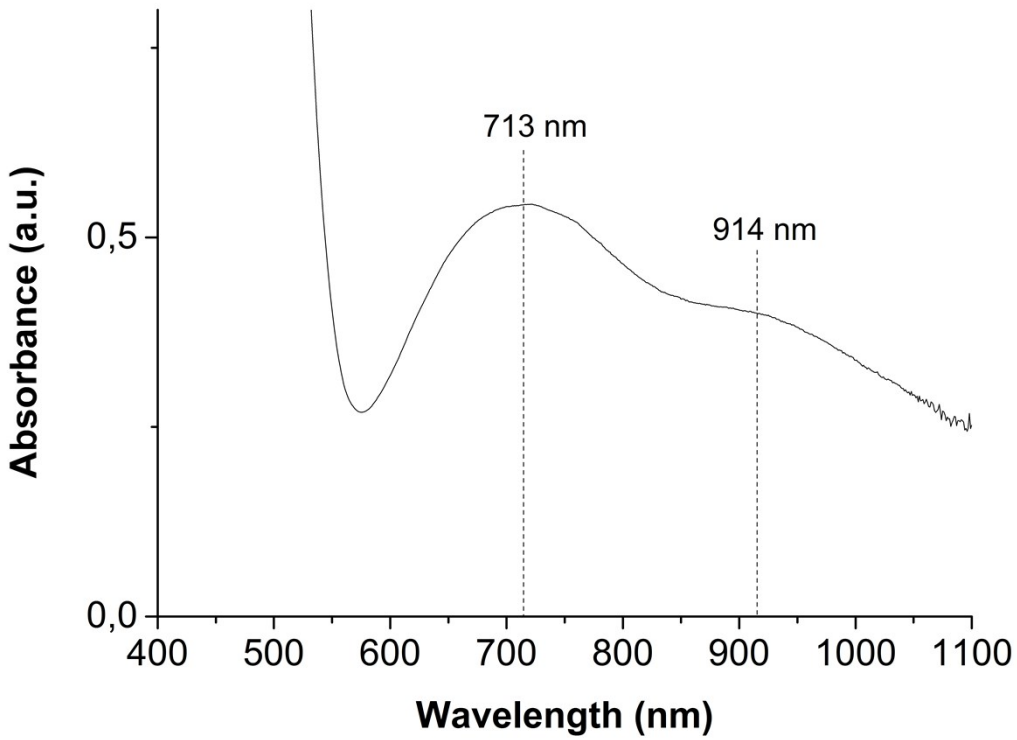

B

Fig. S5: (**A**) UV-Vis spectra of **C0SAL** (2.54 10^{-5} M) in the range 200-400 nm recorded in 24h, each spectrum was acquired every 60 minutes, CH_3CN:H_2O (1:1); (**B**) UV-Vis spectrum of **C0SAL** ($6.49 \cdot 10^{-3}$ M) in the region 400-1100 nm, CH_3CN; 25°C, 1 cm path length.

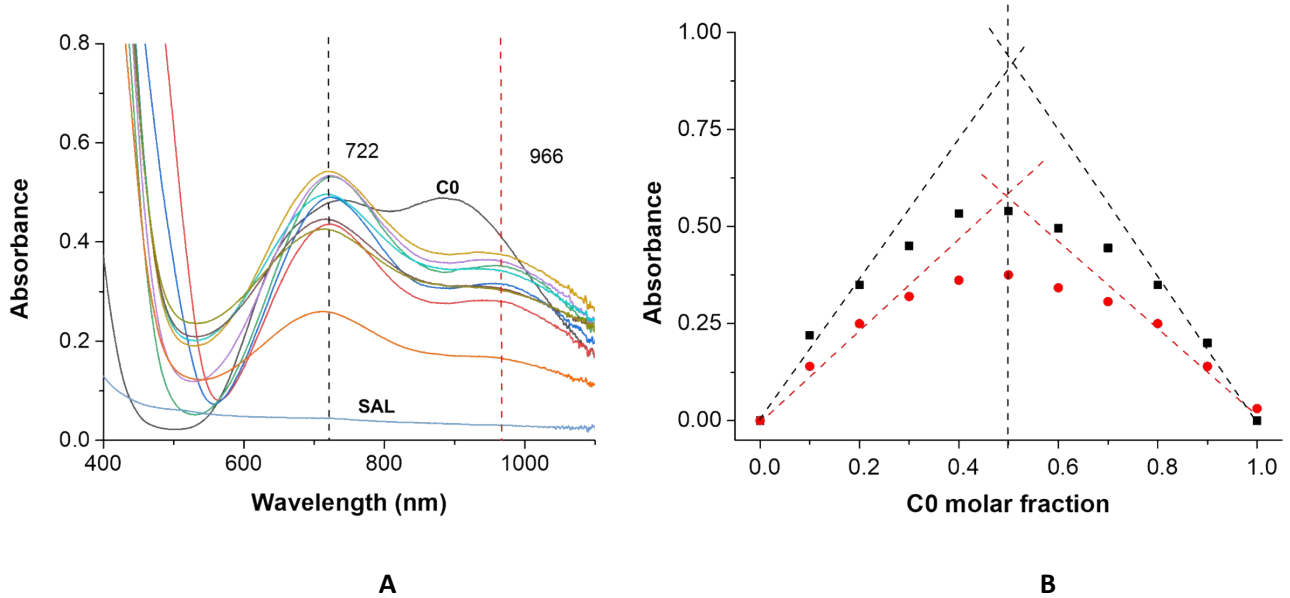

Fig. S6. Absorption spectra collected varying the ligand molar fraction from 0 to 1 for the system between **C0** (1.0 mM) and **SAL** (1.0 mM) in CH_3CN, 0.1 M $NaClO_4$, 25 °C, 1 cm optical path length (**A**). Normalized Job's plot of **C0** and **SAL** at 966 nm (red dots) and 722 nm (black dots).

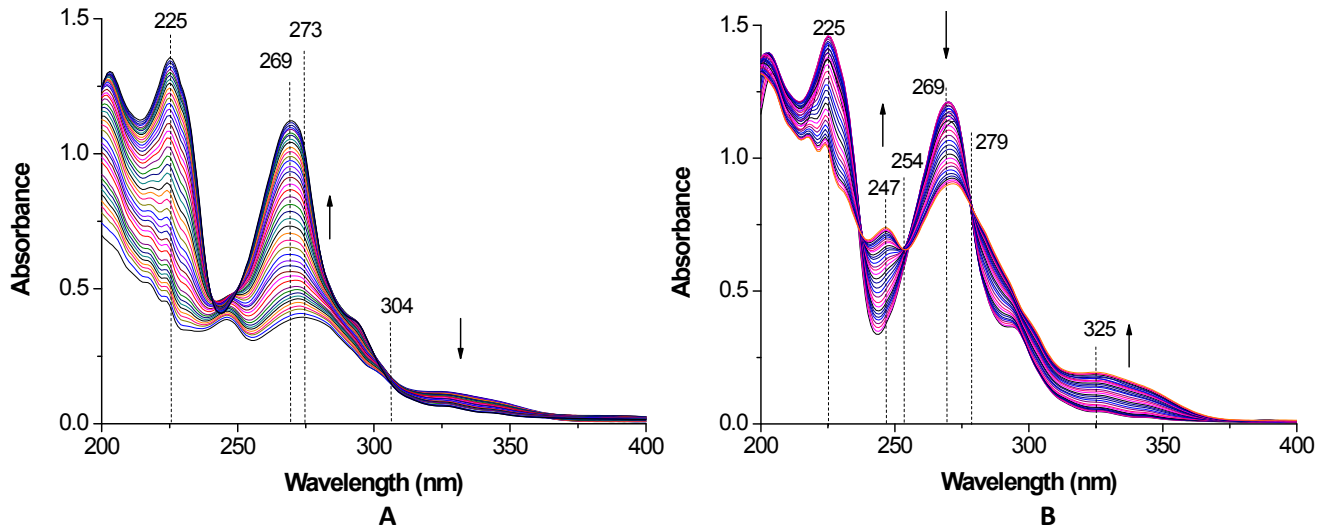

Fig. S7: Selected spectra collected during the titration of $4 \cdot 10^{-5}$ mmoles of **SAL** with **C0** $2 \cdot 10^{-5}$ M (**A**) and of $4 \cdot 10^{-5}$ mmoles of **C0** with **SAL** $4 \cdot 10^{-5}$ M (**B**), CH_3CN, 0.05 M $NaClO_4$ ionic buffer, 25 °C, 1 cm optical path length.

A)

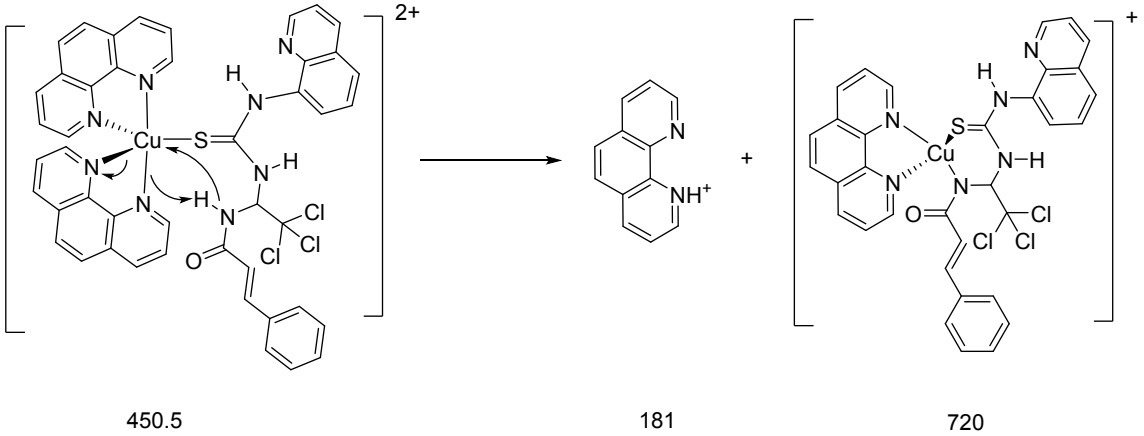

B)

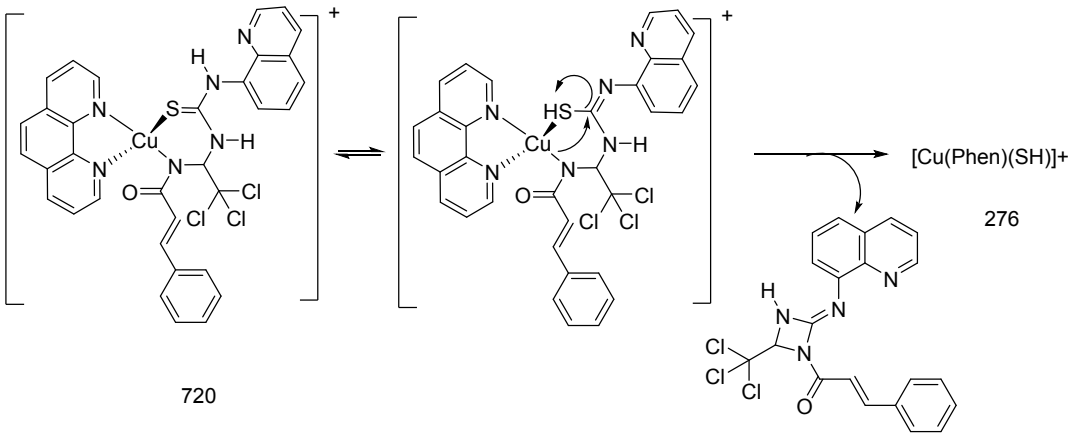

C)

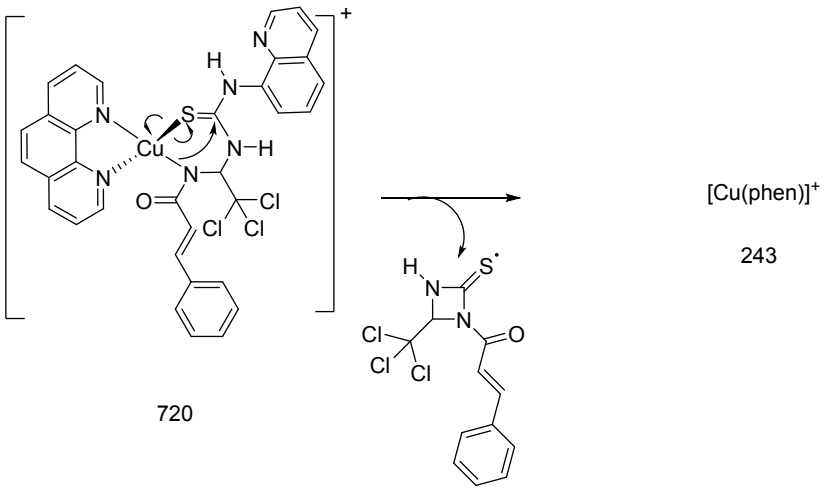

Fig. S8: proposed fragmentation patterns for product ions at 720 (**A**), 276 (**B**), 243 (**C**) *m/z* generated from 450.5 *m/z* under CID conditions.

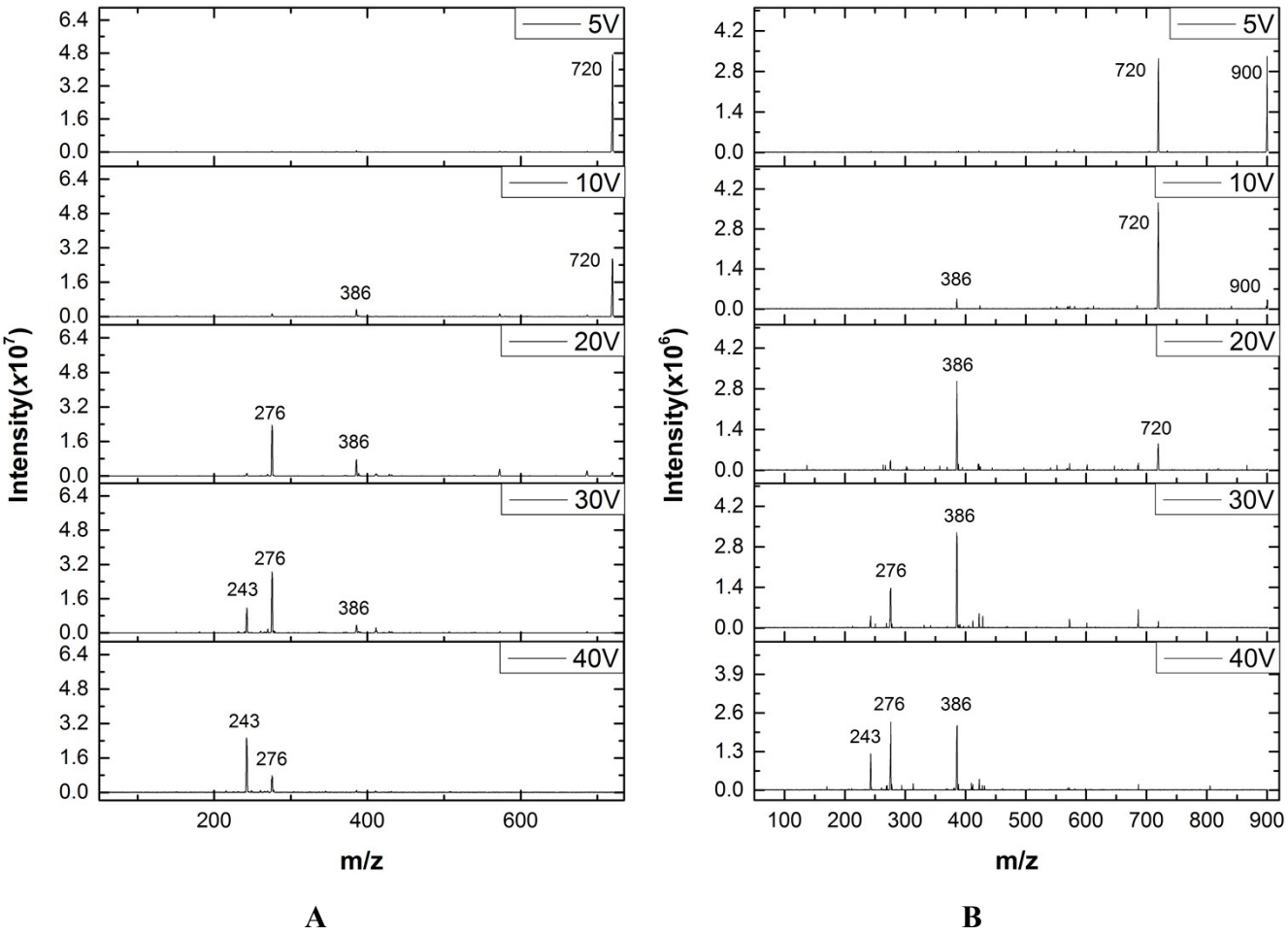

Fig.S9: Tandem mass spectra at different collision energies of (**A**) 720 *m/z* ([Cu(phen)(SAL-H)]$^{+}$) and (**B**) 900 *m/z* ([Cu(phen)$_2$(SAL-H)] $^{+}$).

A)

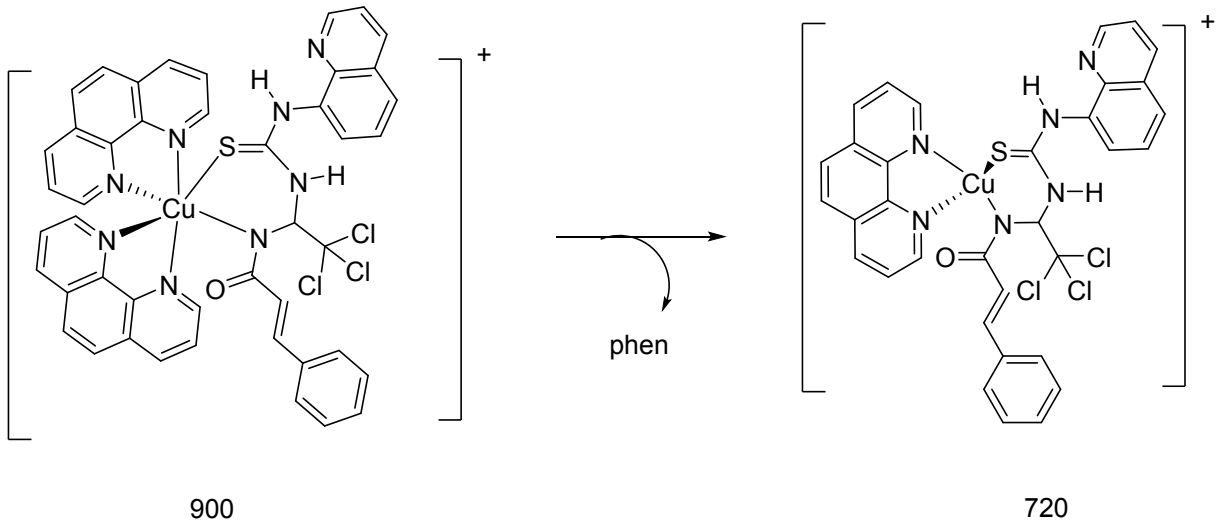

B)

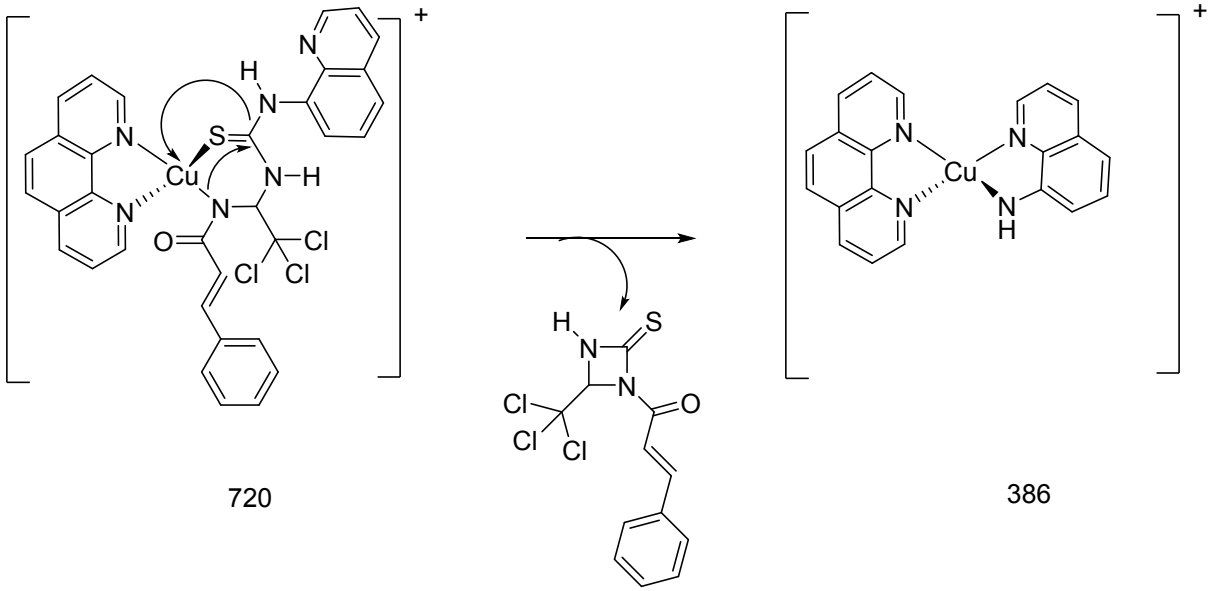

Fig.S10: proposed fragmentation patterns for product ions at 720 (**A**) m/z generated from 900 *m/z*, and for 386 *m/z* (**B**) generated from precursor 720 *m/z* under CID conditions.

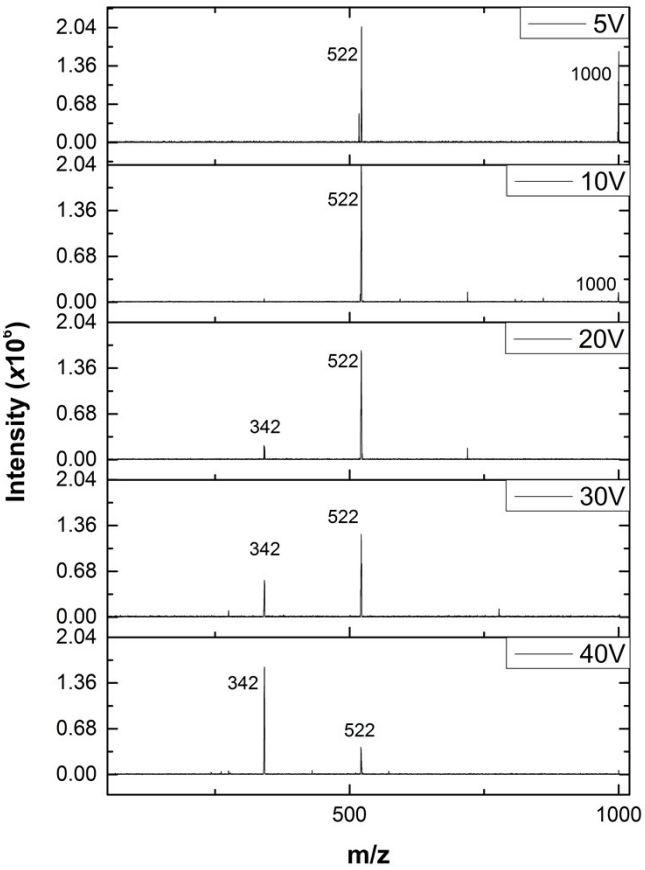

Fig.S11: Tandem mass fragmentation at different collision energies of peak at 1000 *m/z* ($[Cu(phen)_2(SAL)(ClO_4)]^+$).

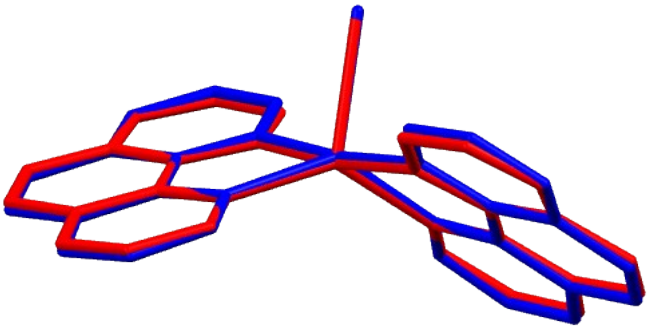

Fig. S12: superimposition of the X-Ray structure (blue coloured) and the DFT optimized structure (red coloured) of $[Cu(phen)_2(H_2O)]^{2+}$. RMSD value obtained for the optimized structure was 0.0905 Å.

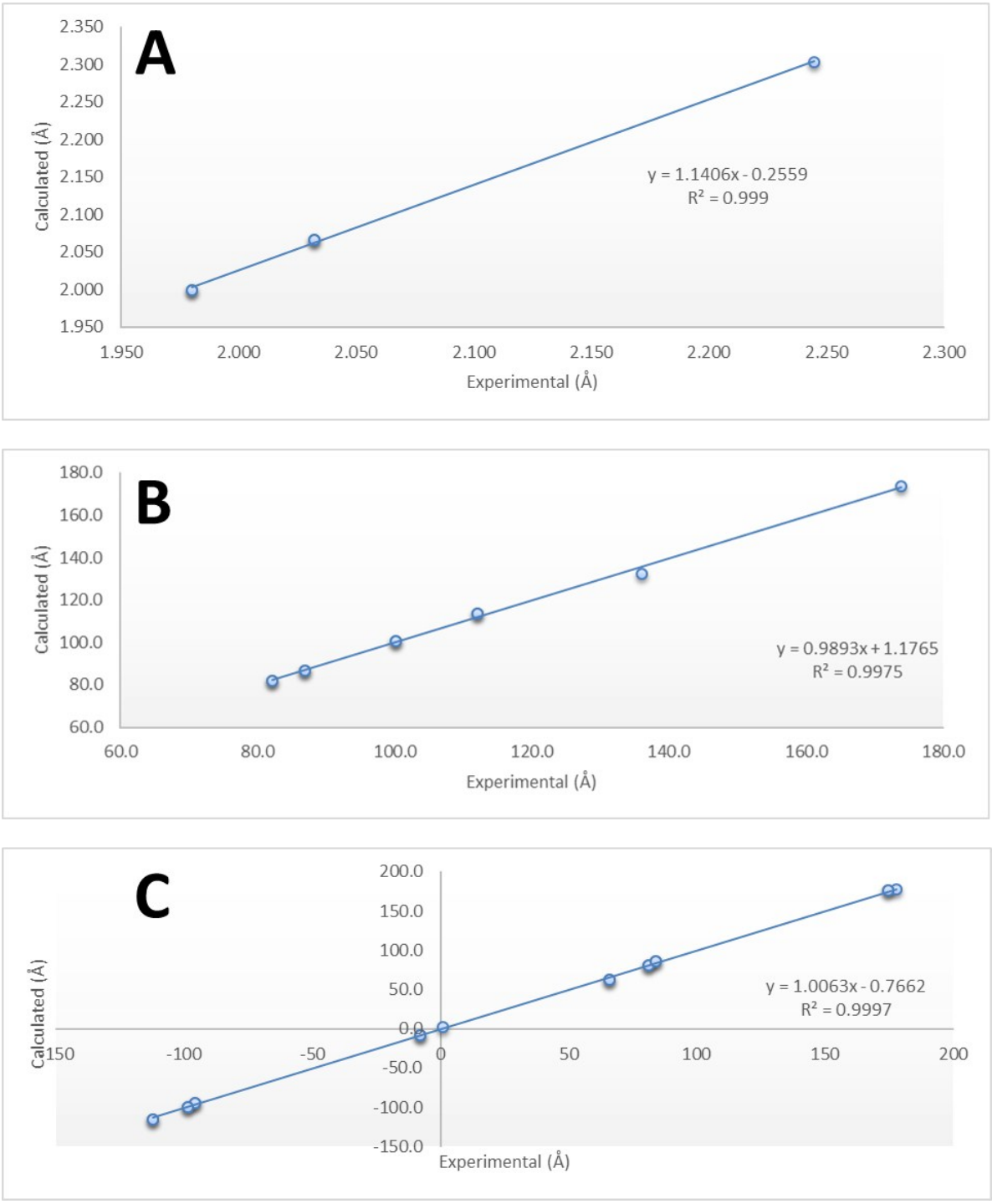

Fig. S13: linear correlation between calculated and experimental bond lengths (**A**), angles (**B**) and dihedrals (**C**) for $[Cu(phen)_2(H_2O)]^{2+}$.

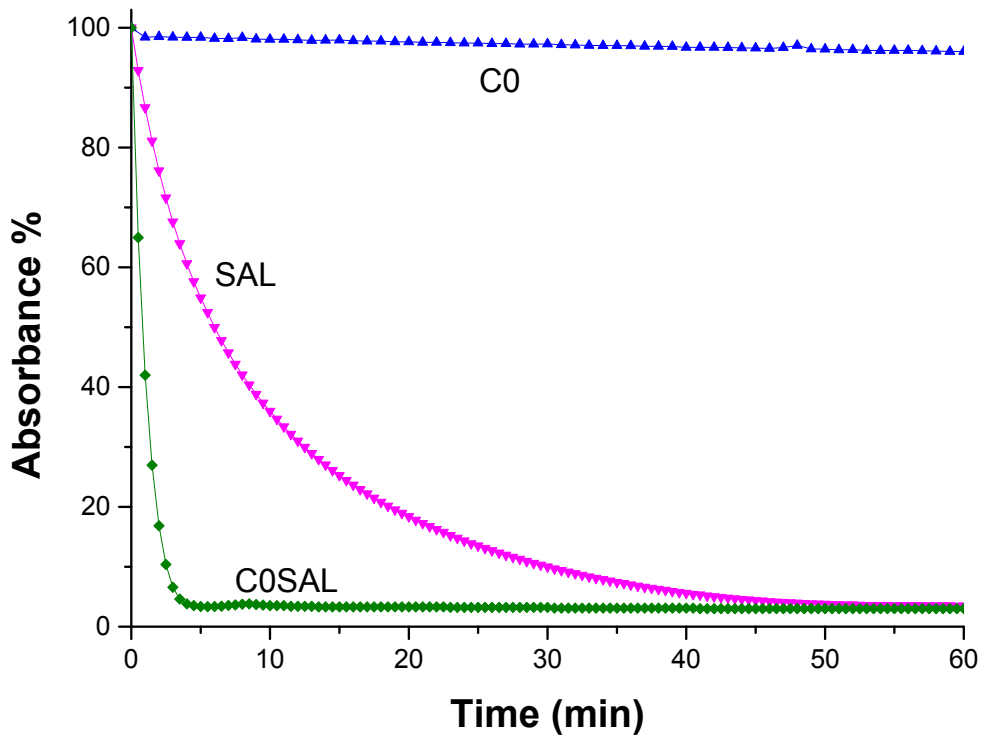

Fig. S14. Reducing activity of DPPH shown by **C0**, **SAL** and **C0SAL** (0.05 mM, absolute ethanol, 25 °C, λ 517 nm).

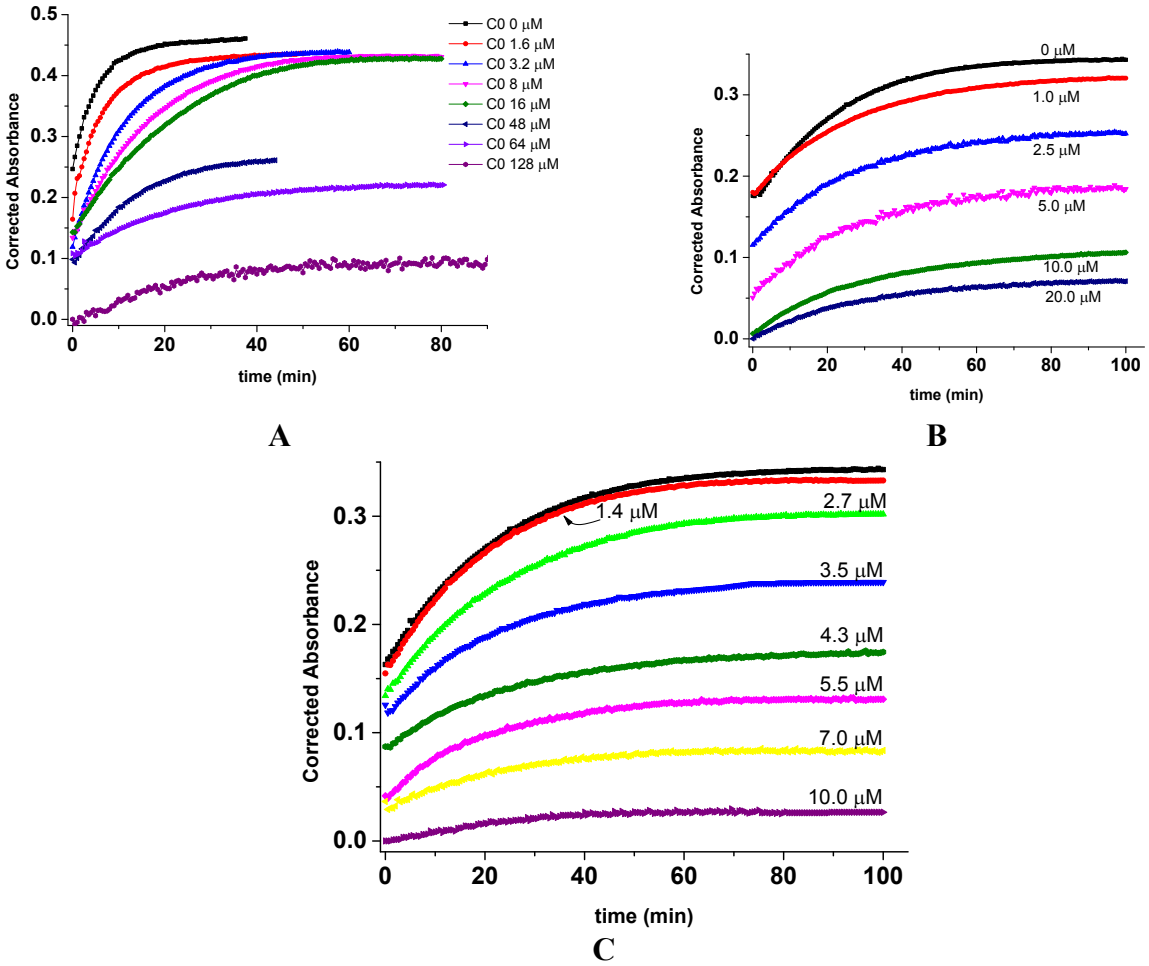

Figure S15. Absorbance at 243 nm of solutions containing linoleic acid, lipoxygenase enzyme and **C0** (**A**) or **SAL** (**B**) or **C0SAL** (**C**) at different molar concentration; linoleic acid 32 μM, lipoxygenase 0.88 nM, pH 7.4 TRIS buffer, T 25°C (values are corrected for the absorbance of **C0SAL**).

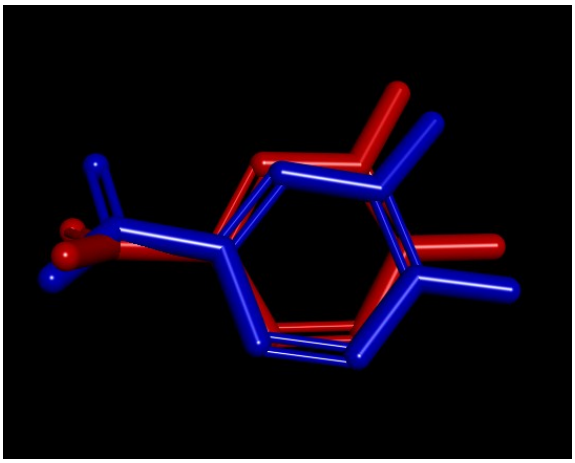

Fig. S16: superimposition of the crystallized pose (blue colored) and the docked pose (red colored) of ligand 3,4-dihydroxybenzoic acid (dhb). RMSD value obtained for the docked pose was 0.6176 Å.

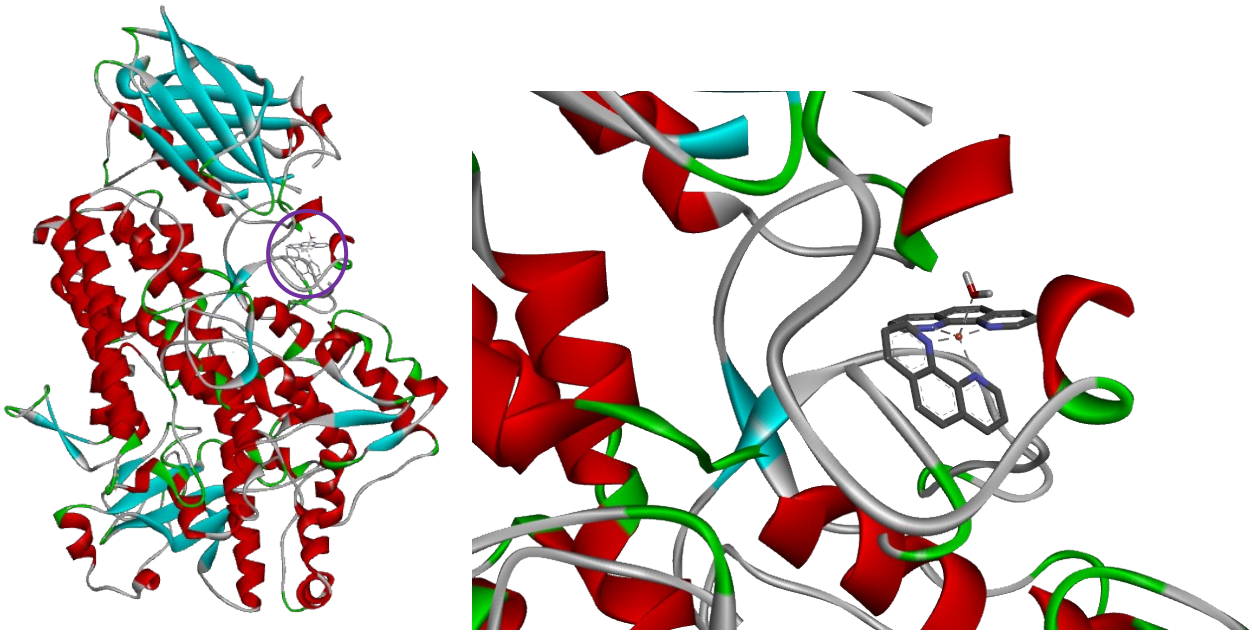

Fig. S17: full view of the complex between the highest-ranking score of $[Cu(phen)_2(H_2O)]^{2+}$ and Soybean LOX (sx); zoom of the binding pocket occupied by the highest ranking score of $[Cu(phen)_2(H_2O)]^{2+}$ and Soybean LOX (dx).

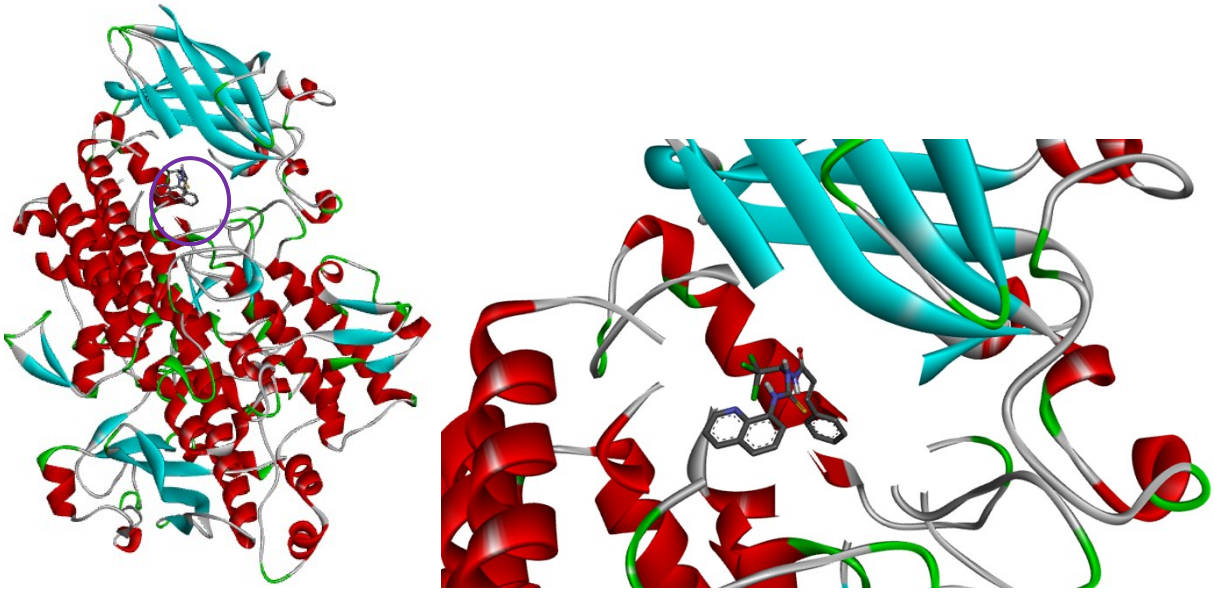

Fig. S18: full view of the complex between the highest-ranking score of SAL and Soybean LOX (sx); zoom of the binding pocket occupied by the highest ranking score of SAL and Soybean LOX (dx).

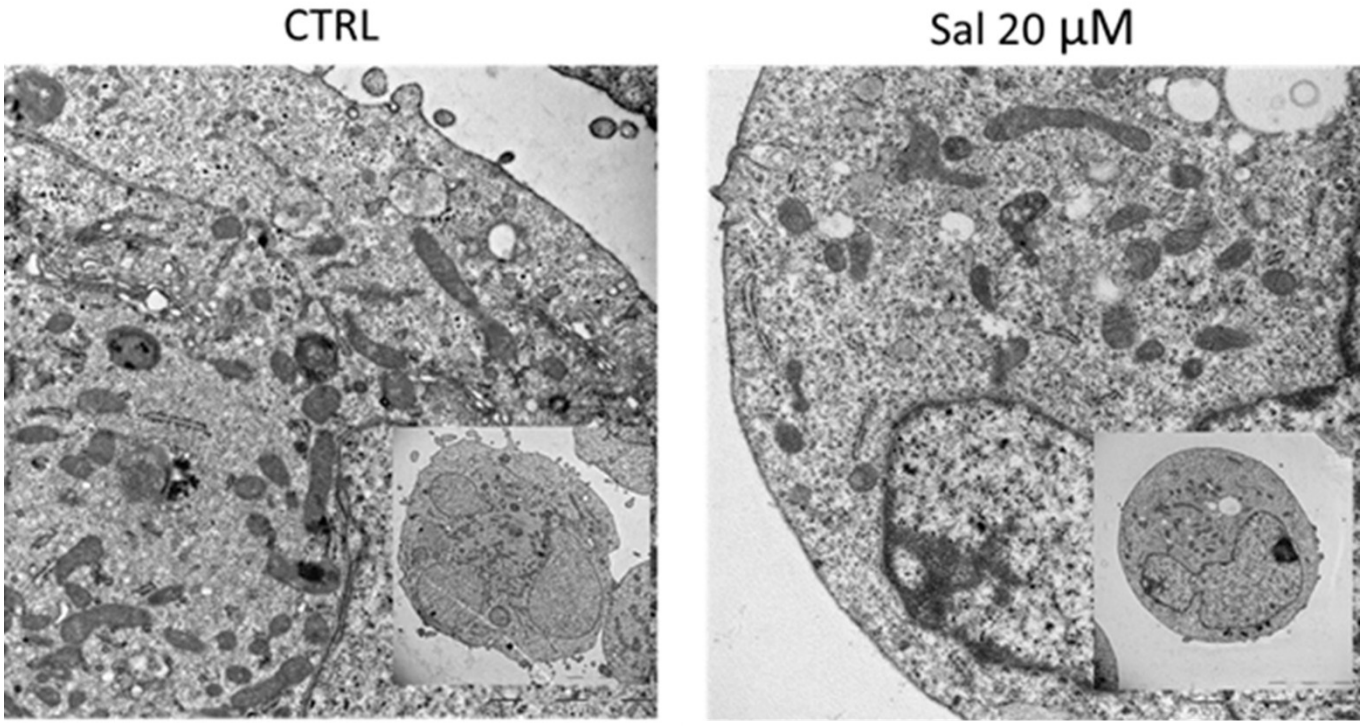

Fig. S19. Transmission electron microscopy (TEM) documenting absence of cytotoxicity in 24 h SAL-treated cells, by visualizing cell ultrastructure. Insets show the overall cell morphology. Scale bars indicate 2 mm.

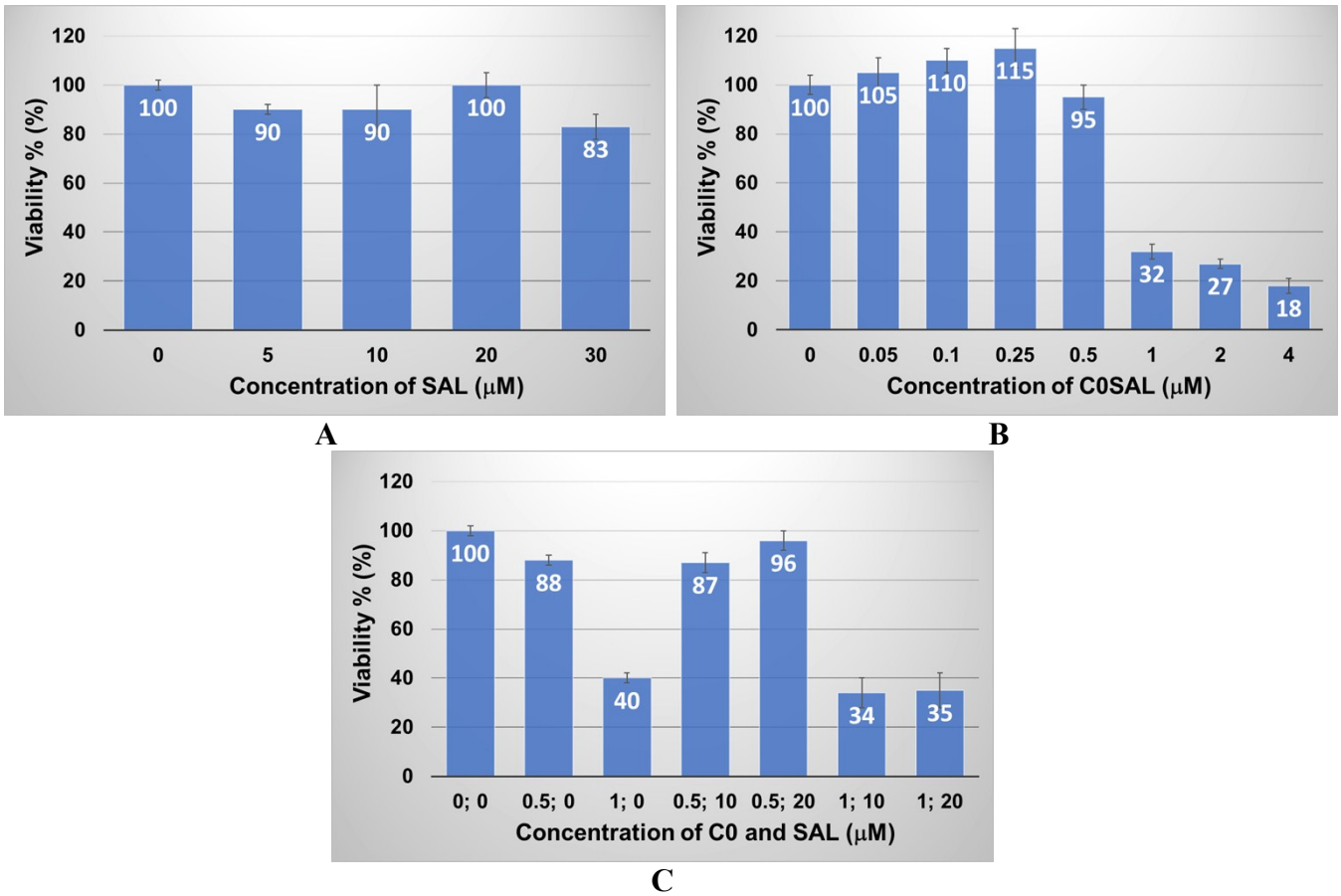

Fig. S20. Viability % of A2780 cells cultured for 24 h in the presence of **SAL** (**A**), **C0** (**B**) and **C0SAL** (**C**). Plots represent means and SD from three independent experiments performed in technical pentaplicates.

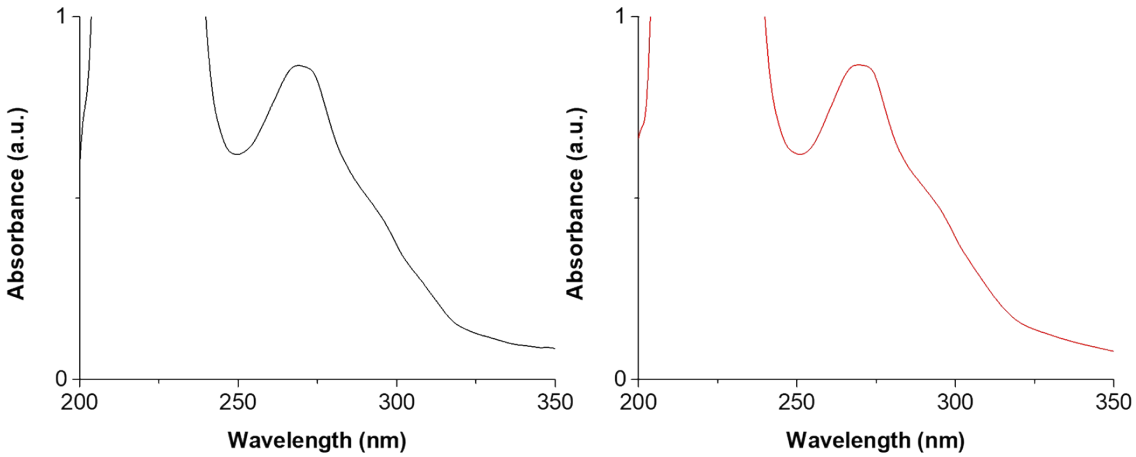

Fig. S21. C0SAL absorption spectrum in DMSO:TRIS (0.5:99.5) freshly prepared (right) and after 48 hrs. (left), C0SAL 10 microM, 1 cm optical path length, 25 °C, pH 7.4 TRIS buffer.

$[Cu(phen)_2(H_2O)]^{2+}$	**DFT**	**Exp.**	$[Cu(phen)_2(H_2O)]^{2+}$	**DFT**	**Exp.**
Cu-O	2.303	2.245	*N1-Cu-N4-C23*	176.5	174.9
Cu-N1	1.999	1.980	*N3-Cu-N2-C10*	-8.3	-7.9
Cu-N2	2.066	2.032	*N3-Cu-N2-C11*	176.6	174.9
Cu-N3	1.999	1.980	*N4-Cu-N2-C10*	80.4	81.4
Cu-N4	2.066	2.032	*N4-Cu-N2-C11*	-94.7	-95.8
N2-Cu-O	113.7	112.0	*N2-Cu-N4-C22*	80.4	81.4
N4-Cu-O	113.8	112.0	*N2-Cu-N4-C23*	-94.7	-95.8
N4-Cu-N2	132.5	136.0	*O-Cu-N1-C1*	62.2	65.9
N1-Cu-O	86.8	86.9	*O-Cu-N1-C12*	-116.3	-112.3
N3-Cu-O	86.8	86.9	*O-Cu-N3-C13*	62.1	65.9
N2-Cu-N1	81.9	82.2	*O-Cu-N3-C24*	-116.4	-112.3
N4-Cu-N3	81.9	82.2	*O-Cu-N2-C10*	-99.6	-98.6
N3-Cu-N1	173.7	173.8	*O-Cu-N2-C11*	85.3	84.2
N3-Cu-N2	100.7	100.1	*O-Cu-N4-C22*	-99.6	-98.6
N4-Cu-N1	100.7	100.1	*O-Cu-N4-C23*	85.3	84.2
N1-Cu-N2-C10	177.5	177.9	*N1-Cu-N4-C22*	-8.3	-7.9
N1-Cu-N2-C11	2.4	0.8	*N1-Cu-N4-C23*	176.5	174.9
N1-Cu-N4-C22	-8.3	-7.9	*N3-Cu-N2-C10*	-8.3	-7.9

Table S1: Selected optimized bond distances (Å), angles (°) and dihedrals (°) for the DFT optimized structure of $[Cu(phen)_2(H_2O)]^{2+}$and the corresponding structural data. Atom labelling scheme as in Figure 4A.

$[Cu(phen)_2(H_2O)]^{2+}$	**Natural charges**
Cu	1.401
N1	-0.519
N2	-0.525
N3	-0.519
N4	-0.525
O	-0.974

Table S2: Selected calculated atomic charges at NPA level for $[Cu(phen)_2(H_2O)]^{2+}$. Atom labelling scheme as in Figure 4A.

SAL	DFT
C9-O	1.223
C9-N1	1.363
C11-Cl1	1.765
C11-Cl2	1.782
C11-Cl3	1.761
N2-C12	1.371
C12-S	1.661
C12-N4	1.353
H10···O	1.938
H10···O-C9	102.4
N1-C10-N2	112.5
N2-C12-S	122.9
N4-C12-S	126.3
N2-C12-N4	110.7
Cl1-C11-C10	107.9
H10···O-C9-N1	-14.2
C9-N1-C10-C11	-96.4
C9-N1-C10-N2	30.1
Cl1-C11-C10-N2	176.5
C1-C11-C10-N1	-56.6

Table S3: Selected optimized bond distances (Å), angles (°) and dihedrals (°) for the DFT optimized structure of **SAL** and corresponding structural data. Atom labelling scheme as in Figure 4B.

[Cu(phen)$_2$(SAL)]$^{2+}$	**DFT**	**[Cu(phen)$_2$(SAL)]$^{2+}$**	**DFT**
Cu-S	2.379	*N3-Cu-N2-C10*	-5.3
Cu-N1	2.014	*N3-Cu-N2-C11*	175.8
Cu-N2	2.184	*N4-Cu-N2-C10*	-87.3
Cu-N3	2.037	*N4-Cu-N2-C11*	93.9
Cu-N4	2.108	*N2-Cu-N4-C22*	-84.9
S-C25	1.712	*N2-Cu-N4-C23*	91.3
N2-Cu-S	105.7	*S-Cu-N1-C1*	-72.3
N4-Cu-S	149.3	*S-Cu-N1-C12*	104.8
N4-Cu-N2	105.0	*S-Cu-N3-C13*	-30.9
N1-Cu-S	89.7	*S-Cu-N3-C24*	154.5
N3-Cu-S	95.6	*S-Cu-N2-C10*	93.0
N2-Cu-N1	79.8	*S-Cu-N2-C11*	-85.9
N4-Cu-N3	80.1	*S-Cu-N4-C22*	94.7
N3-Cu-N1	174.6	*S-Cu-N4-C23*	-89.1
N3-Cu-N2	98.4	*N1-Cu-S-C25*	100.9
N4-Cu-N1	95.4	*N2-Cu-S-C25*	-179.7
Cu-S-C25	108.2	*N3-Cu-S-C25*	-79.4
N1-Cu-N2-C10	179.8	*N4-Cu-S-C25*	0.7
N1-Cu-N2-C11	1.0	*Cu-S-C25-N5*	-149.9
N1-Cu-N4-C22	-4.0	*Cu-S-C25-N6*	32.7
N1-Cu-N4-C23	172.2		

Table S4: Selected optimized bond distances (Å), angles (°) and dihedrals (°) for the DFT optimized structure of [Cu(phen)$_2$(SAL)]$^{2+}$and corresponding structural data. Atom labelling scheme as in Figure 5A.

[Cu(phen)$_2$(SAL)]$^{2+}$	**Natural charges**
Cu	1.280
N1	-0.500
N2	-0.519
N3	-0.520
N4	-0.508
S	-0.267

Table S5: Selected calculated atomic charges at NPA level for [Cu(phen)$_2$(SAL)]$^{2+}$. Atom labelling scheme as in Figure 5A.